Short-range cytokine gradients to mimic paracrine cell interactions *in vitro*

Michael Ansorge[1], Nadine Rastig[1], Ralph Steinborn[1], Tina König[1], Lars Baumann[1], Stephanie Möller[2], Matthias Schnabelrauch[2], Michael Cross[3], Carsten Werner[4,5], Annette Beck-Sickinger[1], Tilo Pompe[1,4,*]

[1] Universität Leipzig, Institute of Biochemistry, Johannisallee 21/23, 04103 Leipzig, Germany
[2] INNOVENT e. V., Biomaterials Department, Prüssingstraße 27B, 07745 Jena, Germany
[3] Universität Leipzig, Department of Hematology, Oncology and Hemostasiology, Johannisallee 32A, 04103 Leipzig, Germany
[4] Leibniz Institute of Polymer Research Dresden, Max Bergmann Center of Biomaterials, Budapester Straße 27, 01069 Dresden, Germany
[5] Technische Universität Dresden, Center for Regenerative Therapies Dresden, Fetscherstraße 105, 01307 Dresden, Germany

* Corresponding author: tilo.pompe@uni-leipzig.de

This article was published in final edited form as:

Ansorge M, Rastig N, Steinborn R, Konig T, Baumann L, Moller S, Schnabelrauch M, Cross M, Werner C, Beck-Sickinger AG, Pompe T. Short-range cytokine gradients to mimic paracrine cell interactions in vitro. J Control Release 224:59-68 (2016).

Abstract

Cell fate decisions in many physiological processes, including embryogenesis, stem cell niche homeostasis and wound healing, are regulated by secretion of small signaling proteins, called cytokines, from source cells to their neighbors or into the environment. Concentration level and steepness of the resulting paracrine gradients elicit different cell responses, including proliferation, differentiation or chemotaxis. For an in-depth analysis of underlying mechanisms, *in vitro* models are required to mimic *in vivo* cytokine gradients. We set up a microparticle-based system to establish short-range cytokine gradients in a three-dimensional extracellular matrix context. To provide native binding sites for cytokines, agarose microparticles were functionalized with different glycosaminoglycans (GAG). After protein was loaded onto microparticles, its slow release was quantified by confocal microscopy and fluorescence correlation spectroscopy. Besides the model protein lysozyme, SDF-1 was used as a relevant chemokine for hematopoietic stem and progenitor cell (HSPC) chemotaxis. For both proteins we found gradients ranging up to 50 µm from the microparticle surface and concentrations in the order of nM to pM in dependence on loading concentration and affinity modulation by the GAG functionalization. Directed chemotactic migration of cells from a hematopoietic cell line (FDCPmix) and primary murine HSPC (Sca-1$^+$ CD150$^+$ CD48$^-$) toward the SDF-1-laden microparticles proved functional short-range gradients in a two-dimensional and three-dimensional setting over time periods of many hours. The approach has the potential to be applied to other cytokines mimicking paracrine cell-cell interactions *in vitro*.

Keywords

gradients, chemokine, chemotaxis, agarose, glycosaminoglycan, microparticle, affinity-based release

Introduction

Cytokines and other small soluble mediator molecules play a crucial role in cell-cell communication of multicellular biological systems. Both long-range (> 100 µm) and short-range gradients of these agents facilitate many cellular processes, including chemotaxis and differentiation during embryogenesis as well as in diseased or regenerating adult tissues. Short-range paracrine interactions between neighboring cells are based on secreted cytokines, which are diluted with increasing distance from the source cells, leading to the establishment of cytokine gradients. Many cellular processes are not sensitive solely to the presence of cytokines, but also to cytokine concentrations or gradients [1,2], so that cell fate decisions frequently depend on the distance between source and receiving cell. As already mentioned, one obvious example is pattern formation during embryogenesis, exemplified by the left-right symmetry created by reaction-diffusion pair Nodal-Lefty [3], or drosophila wing patterning by hedgehog (HH) [4] and decaplentaplegic (Dpp) [5]. However, paracrine signaling also plays a role during wound healing, where platelet-derived growth factor (PDGF) attracts fibroblasts [6] and transforming growth factor-β (TGFβ) induces their transformation into tissue-contracting myofibroblasts [7], as well as in tumor microenvironments [8] and in the regulation of stem cell niches [9]. In these microenvironments stem cell fate is balanced by a multitude of signals including paracrine cytokine gradients from neighboring cells [10,11]. Common examples of these functional entities are the intestinal crypt [12], the hair follicle [13], drosophila testes [14] and the hematopoietic stem cell (HSC) niche in the bone marrow [15,16].

A well-known phenomenon of cellular sensitivity toward cytokine gradients is directed migration of hematopoietic stem and progenitor cells (HSPC) toward gradients of stromal cell-derived factor-1 (SDF-1, also known as CXCL12). This directed movement under the influence of chemokines is referred to as chemotaxis. SDF-1 is a chemokine supporting the homing of HSPC into the bone marrow niche [17], where they show close localization to SDF-1-producing stromal cells [16,18]. SDF-1 acts *via* the G-protein coupled receptor (GPCR) CXC chemokine receptor type 4 (CXCR4) natively expressed on HSPC [19]. Recently the receptor CXC chemokine receptor type 7 (CXCR7) was identified as another target for SDF-1 [20]. It functions mainly as its scavenger thereby modulating cell's mobility [21].

In vivo the presentation, storage and gradient accumulation of many of those cytokines is facilitated by glycosaminoglycans (GAG) – an important component of the extracellular matrix (ECM) [22,23]. These polysaccharides are bound to proteins and besides hydration, their key function is the binding and local concentration of growth factors, cytokines and other mediators [23]. Different configurations and different degrees of sulfation determine cytokine binding, primarily *via* the variable density of negatively charged moieties. While hyaluronan (HA) is the only non-sulfated GAG, heparan sulfate and heparin belong to the most sulfated representatives. Because of this well-documented *in vivo* function the cytokine-GAG interaction has been already used for storage and release systems *in vitro* [24,25].

The high complexity of the *in vivo* tissue microenvironment and stem cell niches established by different cell types, cytokines and the ECM makes analyses and understanding of regulatory processes difficult. Hence, appropriate *in vitro* models are required to mimic physiological processes, including cytokine gradients [26]. Such *in vitro* models permit an in-depth analysis using a multitude of high-resolution techniques. In this way it is possible to get an enhanced understanding of the dynamic processes of disease and tissue development, often exceling static endpoint analysis obtained from *in vivo* experiments [27]. Additionally

such biomimetic *in vitro* models can reduce the number of ethically controversial animal experiments necessary. Several approaches exist for the formation of *in vitro* cytokine gradients. These include traditional methods like transwell assays (based on Boyden chamber) [28], which suffer the disadvantages of ill-defined gradients, endpoint analysis and whole cell population based read-outs. Other approaches use microfluidics to achieve mediator gradients, which can be precisely controlled and enable accurate prediction of a steady-state gradient [29]. However, these methods are frequently limited to long-range gradients over several hundred micrometers [30] and are not suited for mimicking short-range paracrine signals. Furthermore, they are technologically demanding and difficult to set up for multipole, complex spatial arrangements.

We aimed to set up a system to deliver short-range gradients of various mediators in different *in vitro* cell culture environments. The aim was to enable control over cytokine gradients at the cellular scale over several days to investigate cellular processes like migration, proliferation and differentiation. Moreover, the characteristics of the ECM microenvironment should also be controlled in order to better mimic physiological situations of stem cell niches, wound healing or tumor progression. We envisioned an arrangement as depicted in Figure 1 with protein-laden microbeads (µ-beads) as surrogates for cytokine releasing cells and surrounding cells as the receiver of the paracrine signals of interest. Cells and µ-beads are embedded in suitable biomimetic ECM matrices, such as functional three-dimensional (3D) collagen networks as recently introduced [31–33]. Similar µ-beads have already been used as single point sources for proteins, based on either surface-bound [34] or soluble cytokines [6,35,36]. Exemplarily, such a setup should simulate the HSC bone marrow niche with the µ-beads acting as niche cell surrogates in a structured ECM environment similar to that occurring *in vivo*.

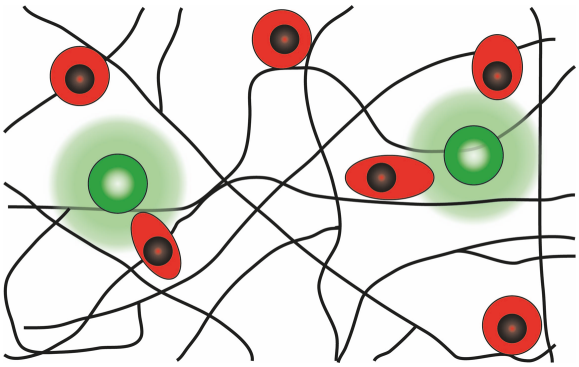

Figure 1: Setup of short-range cytokine gradients from µ-beads to study paracrine cell signals. Protein-laden µ-beads (green) as a local protein delivery vehicle establish short-range, cell-sized protein gradients (pale green) in their proximity due to a slow protein release. Cells (red) and µ-beads are embedded inside a 3D biomimetic ECM network (black lines). Cells in close proximity are able to polarize, migrate, proliferate or differentiate in response to the cytokine gradient. If cells reside far away from the µ-beads and thereby outside the gradient, they will not response (round shape).

Our short-range gradient system was realized by usage of cell-sized spherical agarose µ-beads with different GAG functionalization to control cytokine release. Uptake and release kinetics as well as gradient buildup were quantified from observing fluorescently labeled model proteins including lysozyme and SDF-1 using confocal laser scanning microscopy (cLSM) and fluorescence correlation spectroscopy (FCS). Finally, cell experiments using a

hematopoietic cell line and primary murine hematopoietic stem and progenitor cells (HSPC) proved the presence of functional short-range cytokine gradients by chemotaxis toward SDF-1-laden µ-beads.

Material & methods

Chemicals

Cell culture grade phosphate buffered saline (PBS) was purchased from Biochrom (Berlin, Germany). Bovine serum albumin (BSA, >98 %, M_W = 66 kDa, heat shock fraction), heparin (sodium salt from the porcine intestinal mucosa), lysozyme from chicken hen egg white (>90 %, M_W = 14.3 kDa), monosodium phosphate monobasic monohydrate ($NaH_2PO_4 \cdot H_2O$, BioXtra), sodium phosphate dibasic (Na_2HPO_4, BioXtra), N-(3-dimethylaminopropyl)-N'-ethylcarbodiimide (EDC), N-hydroxysuccinimide (NHS) were all purchased from Sigma-Aldrich (Steinheim, Germany). Sodium bicarbonate ($NaHCO_3$) was purchased from VWR (Darmstadt, Germany), sodium azide (NaN_3, pure), sodium chloride (NaCl, pure) from AppliChem (Darmstadt, Germany), EDC for µ-bead modification from Merck Chemicals (Darmstadt, Germany), rat tail collagen I (4.1 mg/ml, 3298599) from Corning (Amsterdam, Netherlands), and heparin-FITC from Invitrogen (Darmstadt, Germany). All chemicals were used without further purification. Solutions were prepared with deionized water (ρ = 18.2 MΩ).

For µ-bead modification different GAG were used, see also summary in Table 1. Native high molecular weight HA (from *Streptococcus*, average molecular weight as determined with laser light scattering $M_w = 1.1 \cdot 10^6$ g/mol, polydispersity index *PD* = 4.8) was obtained from Aqua Biochem (Dessau, Germany), sulfur trioxide/dimethylformamide complex (SO_3-DMF, purum, ≥ 97%, active SO_3 ≥ 48%) from Fluka Chemie (Buchs, Switzerland). Fluorescence marker (ATTO 565-NH_2) was purchased from ATTO-TEC (Siegen, Germany).

The high-sulfated (hsHA) and the medium-sulfated (msHA) HA derivatives were synthesized and characterized as described previously [37]. Low molecular weight HA was prepared by ozonolysis of high molecular weight native HA. A 1% aqueous solution of high molecular weight HA was treated with ozone, prepared with an ozone generator COM-AD-02 (ANSEROS Klaus Nonnenmacher, Tübingen, Germany) for 2 h. The ozone concentration amounted to approx. 30 g/m^3 and a flow rate of 20 to 30 l/h was used. Finally, N_2 was passed through the solution for 30 min to expel free ozone. The remaining clear solution was dialyzed against distilled water, lyophilized and dried under vacuum. The HA was obtained with 75 to 85% yield. Analytical data of the HA derivatives (HA, hsHA, msHA) are summarized in Table 1.

The functionalization of the HA derivatives (HA, hsHA) with fluorescence dye (ATTO 565-NH_2) was carried out at the reducing end-group of the macromolecules as previously described [38,39]: Briefly, 0.5 mmol of HA and 0.25 mmol of hsHA, respectively, were dissolved in 30 ml of distilled water and the pH value was adjusted with 0.1 M NaOH between 7.5 and 8. Then, 500 µg (0.6 µmol) of the fluorescence marker, dissolved in water, were added to the solution and the reaction mixture was stirred at room temperature (RT) for 6 h. After this time, the pH of the mixtures was adjusted to 7.5 and an equimolar amount of $NaCNBH_3$ (related to GAG) was added in two portions. After stirring at RT for 3 days, the reaction mixture was first dialyzed against deionized water at a pH between 8 and 8.5 and afterwards dialysis was continued against deionized water at pH 5.5 to remove residual

unbound dye. After filtration, lyophilization and drying in vacuum, the labeled GAG were obtained with 85% yield. The msHA was labeled with Atto-565-NH_2 attaching the dye molecules to the carboxylic functions along the polymer chain. A conventional EDC/NHS (Sigma-Aldrich) coupling protocol was used as follows: 0.3 mmol EDC were added to 30 ml of a 10 mM aqueous solution of msHA with a pH of about 4.75. Subsequently, 0.3 mmol NHS were added and the mixture was stirred for 30 min at RT. Then 0.6 µmol of ATTO 565-NH_2, dissolved in water, were added to the polymer mixture and stirred at RT for 6 h. The remaining free carboxyl groups were saturated using ammonia and the solution was stirred for 1 h. After purification as described above the labeled GAG was obtained in 80% yield.

Non-labeled SDF-1 was purchased from Sigma-Aldrich for the 2D cell culture experiments. For the 3D cell culture experiments and protein release analysis, SDF-1 was synthesized by solid phase peptide synthesis as previously described [40]. Fluorescently labeled SDF-1 was synthesized and labeled with the cyanine-based fluorescent label Chromeo 642 (Sigma-Aldrich) specifically attached to alkyne-modified lysine residue (K56) of SDF-1 *via* copper catalyzed click-chemistry as described in detail elsewhere [41]. The K56 does not take part in cell receptor or heparin binding as shown previously for different modifications at position 56 [40,42].

Fibronectin was isolated from adult human blood plasma following the protocol adapted from [43,44].

Table 1: Properties of the different GAG used for µ-bead modification. M_w was determined by laser light scattering (HA, msHA, hsHA) or taken from the manufacturer (heparin). Degree of sulfation (D. S.) was determined by elemental analysis [37] or taken from literature (heparin, [45]).

GAG	M_w / kDa	D. S.	approx. M_w per dimer / Da
HA	23.0	0	400
heparin	18.0	2-3	600
hsHA	21.4	3.8	790
msHA	23.9	2.3	640

Biofunctionalization of microbeads

The cross-linked aminoethyl-modified agarose µ-beads (4% agarose, mean diameter 17 µm, ABT, Madrid, Spain) were modified with the GAG *via* their carboxyl groups using EDC (Merck) according to the manufacturer's instructions. Briefly, 200 µl of the supplied µ-bead suspension were washed three times with water alternated with centrifugation. The respective GAG (heparin, HA, msHA or hsHA, for details see Table 1) was dissolved in the water suspension at a concentration of 3 g/l and EDC was added at a concentration of 20 g/l (0.10 M). The GAG was covalently linked to the µ-beads under constant agitation with an orbital shaker at RT for 4 h. The suspension was then washed with water and subsequently with 1 M sodium chloride (NaCl) to release electrostatically bound GAG, before washing

once more with water. It was finally stored in PBS (150 mM total salt concentration, 12 mM buffer strength) containing 0.02% sodium azide (NaN_3) as preservative at 4 °C. For analyzing the distribution of bound GAG, we used fluorescently labeled derivatives of the respective GAG.

Fluorescent labeling of lysozyme

The fluorescent dye DY-490 (Dyomics, Jena, Germany) and carboxy-tetramethylrhodamine (TAMRA, Biotium, Hayward, USA) were supplied as amine-reactive NHS-esters. The negatively charged fluorescent dye (DY-490) was used because of its high hydrophilicity and low tendency to self-aggregate. However, limited side effects cannot be entirely excluded as the coupling of the negatively charged dye to lysine residues reduces the overall positive net charge of lysozyme. TAMRA was used for control experiments only. Lysozyme was labeled according to the manufacturer's instructions. Briefly, lysozyme was dissolved in PBS and the pH of the solution was adjusted to > 8 using bicarbonate buffer ($NaHCO_3$). The final lysozyme concentration was about 5 mg/ml. The fluorescent dye was dissolved in water-free DMF, immediately before adding it to the protein solution. After a reaction time of around 2 h at RT the solution was fractionated using size exclusion chromatography columns (Sephadex, GE Healthcare). The fractions containing the protein-dye conjugate were pooled and analyzed to determine the protein concentration and degree of labeling using UV/Vis spectrometry (Biophotometer, Eppendorf, Germany).

Bead loading and image acquisition

GAG-functionalized agarose µ-beads were incubated in protein solution with different loading concentrations ranging between 100 and 1000 µg/ml at 4 °C for up to 7 d. In order to measure protein release we used inverted cLSM (LSM 700 or LSM 780, Carl Zeiss, Jena, Germany). To ensure comparability between measurements done on different days, the microscope was switched on at least 4 h before measuring. For measurements, $2 \cdot 10^4$ µ-beads were removed from incubation solution, washed three times in PBS alternated with centrifugation to remove unbound protein and discard it with the supernatant. Afterwards µ-beads were poured into a home-made chamber with glass bottom (#1.5 cover slip, Carl Zeiss) in 1% BSA (Sigma-Aldrich) in PBS to imitate cell culture media conditions. The measurement was started with acquisition of images of the same bead population at time points at 0 h, 24 h and 48 h and additional time points up to 8 d. Between time points the µ-beads were stored at 37 °C to simulate cell culture conditions. We used water immersion objectives (40x/1.2 C-Apochromat or 63x/1.3 LCI-Plan Neofluar, Carl Zeiss) together with highly corrected cover glasses (# 1.5, deviation ± 5 µm) to decrease optical aberrations. Low laser powers (< 2% of a 10 mW diode pumped solid-state laser) were applied to minimize bleaching in combination with a low gain and low resolution to achieve ‘spatial binning’, thereby increasing signal-to-noise ratio. Field illumination was kept homogeneous to ensure constant intensity of excitation light, regardless of the position of the µ-beads in the field of view.

The mean fluorescence intensity (*MFI*) of single µ-beads was analyzed with FIJI (NIH, USA). A binary mask of the µ-bead was created by thresholding (Otsu algorithm) and the *MFI* of the µ-bead was analyzed using the mask area. Using calibration measurements with protein solutions of known concentration, the *MFI* was converted into protein concentration. For

some conditions we had to linearly extrapolate calibration curves to higher concentrations because of protein accumulation inside the µ-beads relative to loading concentrations. This is justifiable as the density of fluorescence label was well below quenching conditions. For each time point 30 to 200 µ-beads (20 images respectively) were analyzed, depending on µ-bead density in the images. The mean of the measured protein concentrations inside each µ-bead was calculated and plotted against the respective time point to yield a release curve.

Theoretical description of protein release and gradient buildup

The obtained time-dependent release data can be described by a diffusion-based approach derived from Fick's second law [46]. A spherical µ-bead's radial symmetry leads to eq. (1) with r being the distance from the center (c local, time-dependent cytokine concentration, D diffusion constant).

$$\frac{\partial c}{\partial t} = D \cdot \left(\frac{\partial^2 c}{\partial r^2} + \frac{2}{r} \frac{\partial c}{\partial r} \right) \tag{1}$$

With boundary conditions of (i) homogeneous initial ($t = 0$) concentration c_0 inside the bead of radius a and (ii) negligible concentration increase far away from the µ-bead (considered as infinite sink) for $t \geq 0$, the solution of eq. (1) for the concentration c in the center of the µ-bead at small time periods (assumed to be valid for t in the order of some days) is [46,47]:

$$\frac{c}{c_0} = \frac{6}{\pi^2} \sum_{n=1}^{\infty} \frac{1}{n^2} \exp\left(-\frac{D_{\mathrm{Bead}} n^2 \pi^2 t}{a^2} \right) \tag{2}$$

With this equation ($n \leq 7$) the cytokine diffusion coefficient inside the µ-bead (D_{Bead}) can be fitted to the measured release curves as a measure of protein mobility inside the µ-beads. The goodness of fit was assessed by coefficient of determination r^2 exceeding 0.8.

A quasi-stationary concentration gradient outside the µ-bead was calculated in a 2D and 3D configuration based on Fick's first law, see [6,46]. We assume (i) an almost constant protein release through the surface of the spherical µ-bead (over short time periods, see results), (ii) a fast buildup of quasi-stationary conditions and (iii) negligible protein accumulation outside the µ-bead in the large cell culture volume. The latter two assumptions are based on the difference in mobility inside and outside the µ-beads, indicated by the cytokine diffusion coefficient inside the µ-bead ($D_{\mathrm{Bead}} \approx 0.1$ µm²/s, see Results and Discussion) and outside the µ-bead ($D_{\mathrm{Solution}} \approx 100$ µm²/s). With these assumptions the concentration gradient around the µ-bead can be calculated with:

$$c_{\mathrm{Gradient}} = \frac{1 \cdot a^3}{3 \cdot D_{\mathrm{Solution}}} \cdot \frac{\Delta c}{\Delta t} \cdot \frac{1}{r} \tag{3}$$

This equation links local protein concentration $c_{\mathrm{Gradient}}(r)$ around a spherical µ-bead of radius a to the release rate of protein from the µ-bead $\Delta c/\Delta t$, which is treated as roughly constant for short time intervals. The release rate is numerically derived from the 1st derivative (slope) of the fit of eq. (2) to the release data at the indicated time point. In a 2D case of protein release from a µ-bead lying on a substrate surface, eq. (3) has to be multiplied by factor of 2 due to mirroring on the substrate surface.

Fluorescence correlation spectroscopy

Release of fluorescently labeled lysozyme was quantified in the vicinity of the µ-beads using fluorescence correlation spectroscopy (FCS) at room temperature. µ-beads were loaded with DY-490-labeled lysozyme at a concentration of 1 mg/ml for one week as described above. After three washing steps with PBS the µ-beads were stored in PBS with 1% BSA and released protein for 24 h. Subsequently the µ-beads were washed again three times with PBS and placed inside the custom-built measuring chamber. Using this experimental setup we determined local concentrations corresponding to protein release rate from the µ-beads after 24 h. The fluctuation over time of fluorescence intensity (ten times for 10 s per position) was recorded at several positions with defined distance to the µ-bead surface up to a distance of 50 µm. The autocorrelation function $G(\tau)$ was determined for τ between 0.2 µs and 3.35 s. Fitting eq. (4) to the autocorrelation function (for τ > 1.2 µs to exclude detector after-pulsing), the molecule number N inside the confocal volume and diffusion time τ_D can be determined [48]:

$$G(\tau) = \frac{1}{\langle N \rangle}\left(1 + \frac{T}{1-T} \cdot e^{\left(-\frac{\tau}{\tau_T}\right)}\right)\left(1 + \frac{\tau}{\tau_D}\right)^{-1}\left(1 + \left(\frac{\omega_0}{z_0}\right)^2 \frac{\tau}{\tau_D}\right)^{-1/2} \quad (4)$$

This approach also accounts for triplet state formation with triplet fraction T (< 0.2) and typical triplet time τ_T (1 to 10 µs). The size of the confocal spot, described by the ratio $\gamma = z_0/\omega_0$ (herein fixed at 6) with the lateral diameter ω_0 and the axial diameter z_0, was determined by FCS analysis of τ_D of a free dye (Atto-488, Atto-Tec) with known diffusion coefficient D_{Dye} (400 µm^2/s) [49] using eq. (5).

$$\omega_0 = \sqrt{4 D_{\mathrm{dye}} \tau_D} \quad (5)$$

Using Atto-488 as calibration standard, we determined τ_D between 22 and 25 µs, correlating to ω_0 of 0.2 µm.

The diffusion coefficient D (eq. (5)) and the concentration c (=N/V) of the lysozyme-dye conjugate was calculated using eq. (5) and (6). For calculating the confocal volume (eq. (6)), it is assumed to be of ellipsoidal shape and was determined to be about 0.2 fl.

$$V = \pi^{3/2} \gamma \omega^3 \quad (6)$$

Cell experiments

The FDCPmix cell line was used because of its known chemotactic response to SDF-1 *via* the CXCR4 receptor [50]. FDCPmix (A4) cells were cultured in maintenance medium [51] based on Iscove`s Modified Dulbecco's Medium (IMDM, Biochrom) with osmolarity adjusted to 0.32 osm/l and supplemented with 5 mM glucose, 2 mM glutamine, 20% donor horse serum and 10% IL-3 conditioned medium [52]. Cells were passaged every two days to a density of $5 \cdot 10^5$ cells/ml. All cells were cultured at 37 °C in 5% CO_2 in air at 95% humidity.

Primary HSPC derived from murine bone marrow were used as an additional model of CXCR4-positive cells. Cells were collected from bone marrow based on SLAM markers according to [27]. Briefly, 1-2 mice (C57/Bl6, 8 weeks old) were killed, femurs and tibias removed, cleaned free of soft tissue, and crushed with a mortar and pestle. The cell suspension in PBS was then filtered and lineage depletion (CD5, CD45R (B220), CD11b, Anti-Gr-1 (Ly-6G/C), 7-4, Ter-119) was performed by magnetic sorting (MACS, Miltenyi,

Bergisch Gladbach, Germany). Staining of Sca-1 (PE) was complemented by anti-CD150 (APC) and anti-CD48 (PerCP/Cy5.5) (all BioLegend, Fell, Germany) staining. Dead cells were identified by propidium iodide (PI, Sigma-Aldrich) staining. Cells were sorted by flow cytometry (FACSAria, BD Biosciences, USA), gating on live, Sca-1^+ and refining for $CD150^+$ and $CD48^-$ to select the long-term repopulating HSPC fraction. After cell sorting HSPC were cultured in StemSpan SCFM (StemCell Technology, Cologne, Germany) supplemented with 10 ng/ml SCF, 10 ng/ml TPO, 20 ng/ml IGF-2, 20 ng/ml FGF-1 (all R&D Systems, Minneapolis, USA), 10 µg/ml heparin (5 kU/ml) and 1% penicillin/streptomycin (both from Biochrom).

Two substrate setups were used to follow chemotaxis of cells. The home-made chamber was either filled with a 3D collagen network or coated with fibronectin on the cover slip base (50 µg/ml in PBS incubated at 37 °C for 1 h). 3D collagen networks were reconstituted according to a recently published protocol [32], using phosphate buffer at pH 8 and collagen I at a concentration of 3 mg/ml to achieve small pore sizes (4 to 10 µm). These networks prevent cells from migrating too fast through the porous network. The µ-beads were incubated in SDF-1 solution at a loading concentration of 10 µg/ml over 2 d. They were washed three times in PBS and put either into the 3D collagen networks during reconstitution or onto the fibronectin-coated surfaces. For control experiments µ-beads without SDF-1 incubation were used.

Cells at a density of $2 \cdot 10^4$ cells/ml were plated onto fibronectin-coated surfaces or on 3D collagen networks. Live cell video microscopy was performed under standard culture conditions (37 °C, 5% CO_2) with a dry objective (20x/0.35 LD A-Plan for 2D experiments or 10x/0.3 EC Plan-Neofluar in combination with 1.6x optovar (all Carl Zeiss) for 3D experiments) over several hours to days (see Results and Discussion). Control experiments were performed under the same conditions using empty µ-beads. For FDCPmix cells on fibronectin-coated surfaces, cells around the µ-beads were counted radially using ImageJ cell counter in FIJI and distance-dependent cell density was calculated by dividing cell number by area of the respective annulus. The cell tracks in 3D experiments were determined manually.

Results and Discussion

µ-bead functionalization with GAG

We aimed to mimic protein secreting cells *via* functionalized cell-sized µ-beads. It is necessary that these beads store and subsequently release cytokines over prolonged periods of time in the order of days. To this end, we utilized native ligands of cytokines in the *in vivo* ECM, namely GAG with different degrees of sulfation in order to adjust cytokine affinity. The linkage of GAG to the aminoethyl-functionalized agarose µ-beads was achieved by EDC-mediated covalent bond formation between the activated acid groups of the GAG (GAG-**COOH**) and the aminoethyl groups of the agarose µ-beads (agarose-CH_2-CH_2-**NH_2**) as sketched in Figure 2A. Due to the porous inner structure of the crosslinked agarose µ-beads, the GAG modification is not restricted to the outer µ-bead region. Images by cLSM, taken at the equatorial plane of the µ-beads with a heparin-FITC functionalization, confirmed the homogeneous heparin distribution inside the bead (Figure 2C). The variations in intensity are due to the porous inner structure of the agarose network. Even after long-term storage (up to one year) at 4 °C we were able to detect a similar amount of fluorescence intensity (data not

shown), indicating stable covalent bond formation, which is consistent with reports available in the literature [53] and from the bead manufacturer (personal communication).

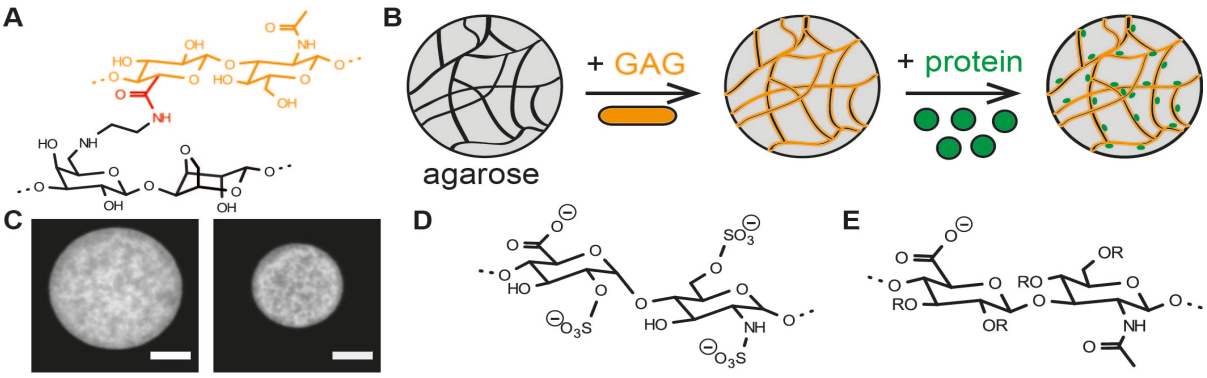

Figure 2: Covalent coupling of GAG to agarose µ-beads. A) The covalent amide bond (red) is formed between the acidic groups of the GAG (orange, here HA) and the amine groups of the agarose (black). **B)** Post-synthetic modification of commercially derived porous agarose µ-beads comprises covalent linkage of GAG (orange) and subsequent cytokine (green) binding due to electrostatic interactions. **C)** Confocal slice through the equatorial plane of a heparin-FITC functionalized agarose µ-bead (left) and of a lysozyme-DY-490 laden µ-bead (right, scale bar: 10 µm). **D)** Structure of a heparin dimer, which consists of 2-O sulfated iduronic acid and 6-O,N-sulfated glucosamine. **E)** Dimeric structure of hyaluronic acid (HA) and its chemically sulfated derivatives, consisting of glucuronic acid and N-acetylglucosamin. For the completely non-sulfated HA the abbreviation R corresponds to a single hydrogen atom. For medium sulfated HA (msHA) and highly sulfated HA (hsHA) 2 R or every R represent a sulfate group, respectively, giving for hsHA a charge density even higher than that of heparin.

After covalent attachment of the GAG, the system is ready for cytokine loading. The dissociation constant K_d of cytokine and GAG as well as the mobility of the cytokine inside the bead pores control cytokine release. The simplified overall reaction scheme is illustrated in Figure 2B: the affinity-based release system contains 3 major components, (i) the inert carrier consisting of crosslinked agarose, with the latter determining the porous structure of the delivery vehicle, (ii) a covalently attached GAG, which provides natural binding sites and determines the affinity for (iii) particular cytokines, chosen to be relevant for the cell system of interest. In contrast to other bead-based release systems made from alginate [35] and sulfated alginate [54], we utilized naturally occurring ligands of the cytokines in the ECM. Non-sulfated and differentially sulfated GAG were applied, as the degree of sulfation is expected to influence cytokine affinity. Using cLSM and fluorimetry in combination with fluorescently labeled derivatives, all GAG species used were shown to bind in a similar manner and density to the agarose µ-beads using EDC chemistry, see e. g. Figure 2C. Heparin usually carries two to three sulfate groups per dimer (Figure 2D) and is the GAG with the highest degree of naturally occurring sulfation. Many cytokines are known to bear heparin binding sites [22,45], so that heparin has an enormous potential to bind cytokines with high affinity. For affinity modulation, chemically modified derivatives of the HA (Figure 2E) were used. The naturally occurring non-sulfated HA provides only weak attraction, while increasing the number of sulfate groups is expected to raise the cytokine affinity accordingly. By modulating the cytokine-GAG affinity, we aimed to alter the initial concentration of cytokine inside the loaded µ-beads as well as the release kinetics.

Modulated release from µ-beads by altered affinity and loading concentration

In a proof of principle release experiment we used fluorescently labeled lysozyme as a model protein because of its high availability, similar size (14.3 kDa) [55] to many cytokines and its net positive charge (pI = 11.35) [56], which is also comparable to many cytokines. We functionalized µ-beads with different GAG (HA, msHA, hsHA, heparin, see Table 1) to modulate protein affinity. Incubation with a lysozyme solution of 1 mg/ml was performed at 4 °C for one week, achieving reproducible loading results after this incubation time (data not shown). The long loading time was used to enable nearly equilibrated protein binding to GAG binding sites. Our results (Figure 3A) support the two main hypotheses, that the system employed enables (i) a slow lysozyme release over a period of days and (ii) a release modulation through GAG-functionalization. All sulfated GAG (heparin, hsHA, msHA) allow for high initial loading of the µ-beads in the range of 1 to 2 mg/ml. After a fast drop in lysozyme concentration inside the µ-beads during the first 24 h, a small but sustained release is observed over several days. This release behavior can be described by the diffusion model depicted in eq. (2). A fit of the model to the data reveals a diffusion coefficient inside the µ-beads D_{Bead} of roughly 4×10^{-5} µm^2/s (

Table 2). This diffusion coefficient is six orders of magnitude smaller than D for free diffusion of lysozyme, which is about 100 µm^2/s [57]. This result justifies the assumption made in our diffusion-based release model, namely that of a much lower cytokine mobility inside the µ-bead in comparison to free diffusion outside the µ-bead.

Table 2: Parameters of lysozyme release modulated by GAG affinity and loading concentration.

GAG	c_0 in mg/ml	D_{Bead} in 10^{-5} µm^2/s (mean ± SEM)	$\Delta c/\Delta t$ after 24 h in ng/(ml·s)
HA	0.6	---*	---*
Heparin	1.3	4.1 ± 0.8	1.3
hsHA	1.6	4.2 ± 1.1	1.5
msHA	1.8	3.7 ± 1.0	1.2

SEM – standard error of the mean. * no significant release detected, therefore not determined. D_{Bead} and $\Delta c/\Delta t$ were determined from fit of eq. (2) to the release data (see Figure 3A), based on at least 68 individual beads per time point.

The low lysozyme mobility inside the µ-beads suggests the following release mechanisms: The crosslinked agarose is considered to be a porous network with negligible influence on cytokine mobility due to the very small size (a few nm) of lysozyme in comparison to the network pores (150 to 200 nm, according to the bead manufacturer, personal communication). The reduction of lysozyme mobility inside the agarose µ-beads is caused by the GAG-functionalization, providing highly charged but non-specific binding sites which enable continuous re-binding after dissociation. This results in a decreased diffusion coefficient determined by the fit (eq. (2)). Hence, inside the µ-bead we have a quasi-static equilibrium between a small unbound and a large bound fraction of protein. The unbound

protein concentration should drop drastically at the bead surface, because of its release into the surrounding medium. The binding and release of protein to and from the GAG is influenced by the mutual affinity and the availability of free binding sites, as will be shown below.

The functionalization of µ-beads with HA instead of sulfated GAG showed the modulation of loading and release of lysozyme reflecting its affinity for GAG. A much lower initial concentration of lysozyme (c_0 = 0.6 mg/ml), even smaller than c_{Load}, and almost no release were found for HA functionalization (Figure 3A). A similar dependence on the degree of sulfation was recently reported for TGFβ with the highest initial concentration for highly sulfated HA [58]. We did not find strong differences in lysozyme mobility (D_{Bead}) or release rates after 24 h and 72 h dependent on GAG-functionalization. Presumably this behavior is caused by similar release mechanisms for all µ-bead modifications, driven by the strong concentration gradient at the bead surface. This concentration difference at the µ-bead surface is of the same order of magnitude for all experimental settings. For simplification we do not consider additional effects due to proteolysis during the time period of the experiment. This is reasonable as GAG-facilitated protection from degradation can be assumed for proteins in the bound state [23]. In all experiments we find a considerable high fraction of immobile lysozyme inside the µ-beads (> 50% of c_0) which we attribute to strong electrostatic interactions between negatively charged GAG and positively charged lysozyme, usually observed in these release systems [24,35]. GAG binding is able to reversibly change protein conformation (to maximize free binding enthalpy) [59], but released cytokines keep their biological functionality [25,60]. We cannot exclude some irreversible binding events and reversible binding with subsequent loss of functionality [61]. However, our functional cell experiments shown below demonstrate functional proteins released from the µ-beads over long times.

Cytokine release depends on the affinity to the GAG used for functionalization, but also on the loading concentration. Figure 3B shows the dependence of c_0 on the loading concentration c_{Load} for hsHA-functionalized µ-beads as an example. In comparison to Figure 3A the concentration of protein initially bound inside the µ-bead is lower than c_{Load} due to the shortened incubation time of 24 h. We found an almost linear correlation of c_0 and c_{Load} with no saturation even at high c_{Load}. These results indicate that the GAG-functionalization of the agarose µ-beads provides a large number of binding sites for the cytokines that do not approach saturation at our loading concentrations. This also supports our proposed release mechanism with a quasi-static equilibrium of bound and unbound protein inside the µ-beads with many free binding sites available. The similar D_{Bead} in the release kinetics independent of c_0 is also consistent with this idea (data not shown).

Determination of the very low lysozyme concentration in the surrounding medium around the µ-beads was not possible with the cLSM setup, confirming reports by other groups [35]. However, the resulting cytokine gradients, which cells are able to detect, can be calculated with an analytical solution assuming a nearly constant protein release rate from the µ-bead, see eq. (3) in Material and Methods section. This solution holds true for single point sources, namely individual and well-separated µ-beads and measurements far away from the µ-bead surface, and a low rate of protein release, insufficient to generate considerable increase in protein concentration far away from the µ-beads over time.

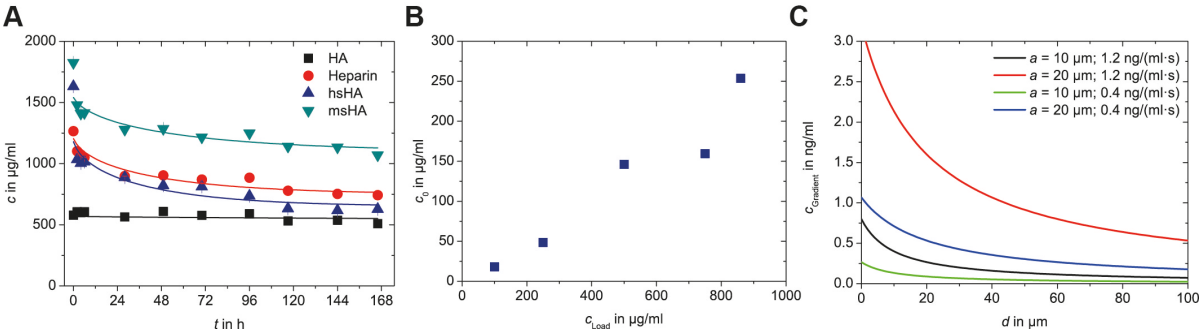

Figure 3: Modulation of lysozyme release by affinity and loading concentration. A) Lysozyme release from GAG-functionalized µ-beads determined over a time period of one week in dependence on GAG functionalization. Solid lines correspond to fits of the release data by the diffusion-based approach (eq. 2, mean bead radius *a* = 10 µm). Data are shown as mean ± standard error of the mean (SEM). Each data point represents *MFI* of at least 68 µ-beads. *MFI* was related to concentration *via* calibration measurements of known lysozyme solutions. The incubation time of µ-beads was 7 d at a loading concentration of 1 mg/ml. **B)** Initial concentration c_0 (at t = 0) of lysozyme inside the µ-beads in dependence on loading concentration c_{Load}. Data are shown as described in **A)** from at least 40 µ-beads. An incubation time of 24 h was used. **C)** Expected short-range gradients of lysozyme with increasing distance *d* from µ-beads surface. The concentrations are calculated for indicated bead radius *a* and release rates, depending on the time point of release. The release rates correlate to measurements in **A)** and **B)**. Release rates of 1.2 ng/(ml·s) and 0.4 ng/(ml·s) correspond to time points 24 h and 72 h after start of release, respectively.

We calculated lysozyme gradients using release rates ($\Delta c/\Delta t$) determined from the measurements in Figure 3A, see also

Table 2. The results show that we should be able to construct short-range gradients with concentrations of about 50 pM (0.5 ng/ml) at a distance of 50 µm (also depending on the mean bead radius *a* as indicated in Figure 3C). The concentration drops further to 10 pM (0.1 ng/ml) over the next 50 µm, farther away from the µ-bead surface. Variation of GAG-affinity, loading concentration or bead radius allows for the modulation of the release rate and the resulting concentration levels of the established gradients. Over longer time periods (> 3 days) our system provides constant release rates in the range of 0.4 ng/(ml·s), which correspond to gradients in the lower pM range. As a consequence we expect short-range cytokine gradients from 100 pM to 10 pM levels at distances of 10 to 100 µm from the µ-beads, sufficient for cells to sense [1].

Experimental verification of short-range protein gradients

To verify our calculated short-range gradients based on the release data, we utilized fluorescence correlation spectroscopy (FCS) to determine the low protein concentration directly in the vicinity of the µ-bead. Again, these measurements were carried out using fluorescently labeled lysozyme as a model protein.

We performed single point FCS measurements at different positions with increasing distance from the µ-bead surface from 5 µm to 50 µm (Figure 4A). The quantification of lysozyme concentration was achieved by means of the autocorrelation curve, derived from the temporal intensity fluctuations. At τ = 0 one can extract to number of the fluorescent particles inside the confocal volume. An example for an autocorrelation curve at a position 13 µm

away from the µ-bead surface is given in Figure 4B. The particle number of $N = 0.185$ corresponds to a concentration of 1.5 nM. The respective diffusion time of 65 µs equals a diffusion coefficient of 120 µm^2/s, which is in accordance with a theoretically obtained and experimentally proved diffusion coefficient of lysozyme in solution of around 100 µm^2/s [57].

As expected the measured local concentrations drop with increasing distance (Figure 4C), nicely proving the gradient nature of the protein release. Concentrations next to µ-beads are higher and the gradient is stronger than predicted from the steady-state release model (eq. (3)). We mainly attribute this to perturbations of FCS measurements in the proximity of the highly loaded µ-bead by the high fluorochrome concentrations. Deviations might also result from the steady-state solution of protein diffusion not taking into account the details of the µ-bead surface crossing. This discrepancy awaits further investigation. At larger distances (> 70 µm), no detailed comparison of model and experiment is possible as the predicted concentration drops below the quantitation limit of FCS using these settings. However, at intermediate distance (15 µm < d < 70 µm) the model predictions of eq. (3) fit the experimental data and our cell experiments nicely proof the established gradients (see below).

In summary, these results demonstrate the formation of short-range cytokine gradients in the range of 10 to 50 µm, validate their estimation *via* quantification of protein release from the µ-beads, and thus advocate the application of this system in cell experiments.

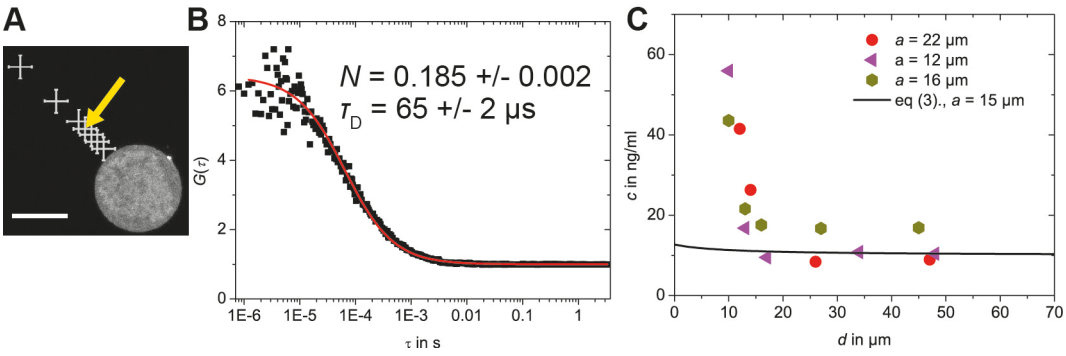

Figure 4: Verification of short-range gradients by FCS. A) Example of FCS measurement points (crosses) with increasing distance from the bead surface. The bead radius a was 15.5 µm and the yellow arrow indicates position of the measuring point for determined autocorrelation function shown in **B**) (scale bar: 20 µm). **B)** Autocorrelation function $G(\tau)$ from position as indicated in **A)**. The red line is the resulting fit using eq. 4. The determined number of fluorescent proteins in the confocal volume N corresponds to a concentration of 1.5 nM or 22 ng/ml of lysozyme. **C)** The measurements of local concentration at distance d from the µ-bead confirm short-range gradients within a distance of 10 to 40 µm. The solid line indicates the calculated gradient determined with eq. (3) (2D case) based on the experimental release data (here 1.2 ng/(ml·s)).

Chemotaxis of hematopoietic stem and progenitor cells in local SDF-1 gradients

After setting up the short-range gradient system using the model protein lysozyme, we chose the cytokine SDF-1 as a well-known example to functionally validate our system using cultured cells. SDF-1 is a chemokine known to act on the CXCR4 receptor present on HSPC and to have an important function in homing of HSPC to the bone marrow niche [17]. With

loading and subsequent release of SDF-1 we expect chemotaxis of HSPC toward the µ-beads, providing a straightforward experimental read-out.

First we determined the release kinetics of SDF-1 from heparin-functionalized µ-beads. The fluorescent label was attached specifically to a non-essential lysine residue (K56) [40–42], so that SDF-1-heparin binding can be assumed not to be biased by the fluorescent label. Loading concentrations of 10, 20 and 30 µg/ml SDF-1 were chosen according to release data from other heparin-based systems available in the literature [25,60]. Our results (Figure 5A&B) confirm the predictability of our system: (i) high SDF-1 accumulation in the µ-beads and (ii) slow release of SDF-1 from the µ-beads, indicating high affinity binding of SDF-1 to heparin-functionalized µ-beads. This was to be expected, because of the specific interaction of heparin with the respective binding site on SDF-1 [62]. The initial SDF-1 concentration inside the µ-beads c_0 correlated almost linearly with the loading concentration c_{Load} as had been found for lysozyme (Figure 5C). The fourfold enrichment found comparing c_{Load} and c_0, was much higher than that for lysozyme. From the fits of eq. (2) to the SDF-1 release data, SDF-1 mobility inside the µ-beads (D_{Bead}) was around 8×10^{-5} µm^2/s and therefore in the same range as for lysozyme. This finding again supports the idea that cytokine release from the µ-beads is predominantly influenced by the strong drop in unbound cytokine concentration at the µ-bead surface.

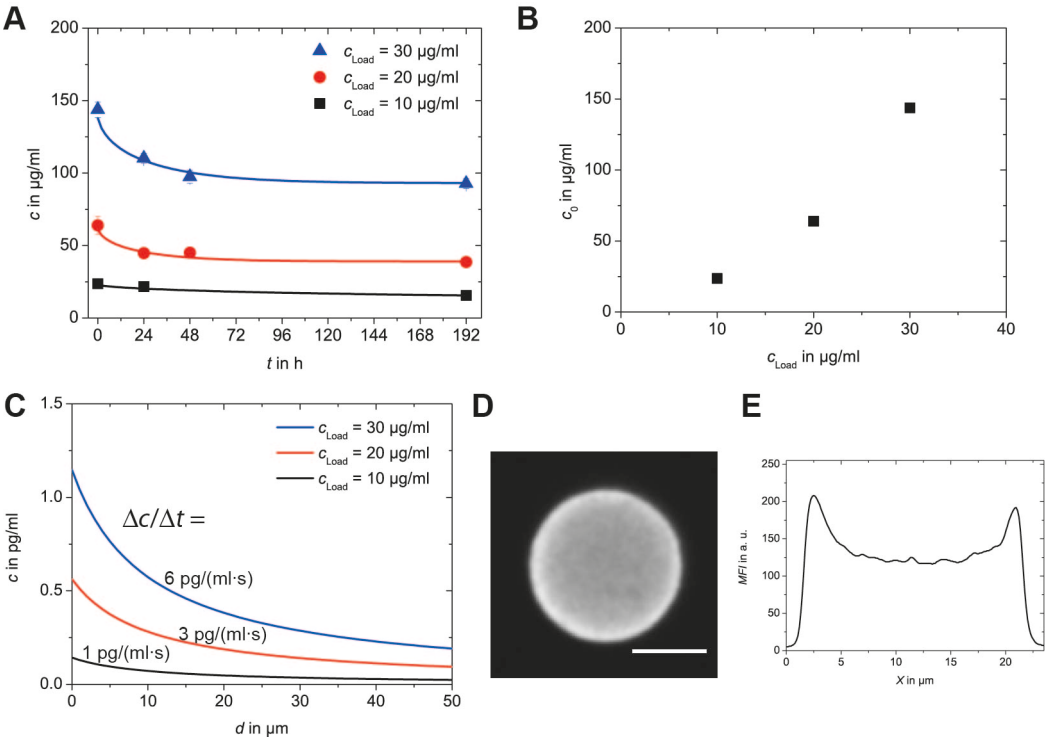

Figure 5: SDF-1 release from heparin-functionalized µ-beads. A) Release kinetics of SDF-1 from µ-beads over several days with different SDF-1 loading concentrations c_{Load}. Solid lines correspond to fits of the release data by the diffusion-based approach (eq. (2), mean bead radius a = 10 µm). Data are presented as mean ± standard error (SEM). Each data point represents *MFI* of at least 30 µ-beads. *MFI* was related to SDF-1 concentration *via* calibration measurements of known SDF-1 solutions. **B)** Initial concentration c_0 (at t = 0) of SDF-1 inside the µ-beads in dependence on loading concentration c_{Load} from measurements in **A)**. **C)** Resulting short-range gradient in 3D after 24 h around the µ-beads calculated from eq. (3). The release rates (indicated at each line) were taken from the fit at 24 h in **A)**, assuming mean bead radius a of 10 µm. **D)** cLSM image at the equatorial plane of

a heparin-functionalized µ-bead illustrates homogeneous initial distribution of fluorescently labeled SDF-1 (scale bar: 10 µm). **E)** A cross-section intensity profile of the µ-bead in **D)** shows intensity maxima at the outer border of the µ-bead.

The observed local accumulation of SDF-1 at the µ-bead surface (Figure 5D&E) probably results from the fluorescent dye. Although some reports suggest that this phenomenon can be caused by charged molecules (positively-charged SDF-1 entrapped at counter-charged pore walls based on negatively-charged heparin [63]), our data indicate a dye artifact. Using lysozyme labeled with the hydrophilic DY-490, no protein accumulation was observed at the µ-bead surface (see Figure 2C). In contrast, control experiments using a rhodamine-labeled (TAMRA) lysozyme showed protein accumulation at the µ-bead surface similar to that seen with SDF-1 (data not shown). Hydrophobic interactions at high concentrations between rhodamine or cyanine dyes (the latter were used for SDF-1) may therefore explain the observed accumulation at the µ-bead surface.

The experimentally obtained release rates after 24 h (around 5 pg/(ml·s), depending on the loading concentration) were used to determine the SDF-1 gradient in the area surrounding the µ-bead based on eq. (3) (Figure 5C). Gradients on a level of 0.1 pM are achieved within 50 µm distance of the µ-beads, which should be sufficient to provide short-range SDF-1 gradients to be detected by HSPC. The measured release rates of 5 pg/(ml·s) (corresponding to 10^{-7} ng/h) are comparable to cell secretion data of SDF-1 (estimated to a single cell secretion of about 10^{-7} ng/h) [64] and to reports of very low SDF-1 release (< 10^{-5} ng/h) from alginate beads [35].

Because the level of SDF-1 in the blood stem cell niche is still unknown, cell experiments are necessary to clarify whether cells can sense low pM concentrations and respond with directed movement toward the chemokine source. However, it is known, that eukaryotic cells can sense very shallow gradients to perform chemotaxis [65]. To test our system we used FDCPmix cells as a surrogate of HSPC, because they also bear the CXCR4 receptor, needed for SDF-1 sensing [50]. As expected SDF-1 laden µ-beads induced chemotaxis toward the chemokine source on a fibronectin-coated surface, whereas no directed cell movement was observed with the empty µ-beads (Figure 6A). These observations show cytokine stability inside the µ-beads and underline the retained biological function after chemokine release. We quantified cell density with respect to distance from the µ-bead surface for different time points (Figure 6B). The data clearly show the time-dependent accumulation of FDCPmix cells next to the µ-beads. This accumulating effect could be observed up to a distance of 40 µm away from the µ-bead surface. When we relate this distance to our calculated gradients it suggests that FDCPmix cells can sense gradients down to a concentration of 2 pg/ml ($\Delta c/\Delta t \approx 1$ ng/(ml·s) for these early time points of SDF-1 release). Hence, these experiments prove the functionality of the established cytokine gradients along with their short-range character with some tens of µm range and allow us to rule out unspecific attraction by the unloaded GAG-functionalized µ-beads.

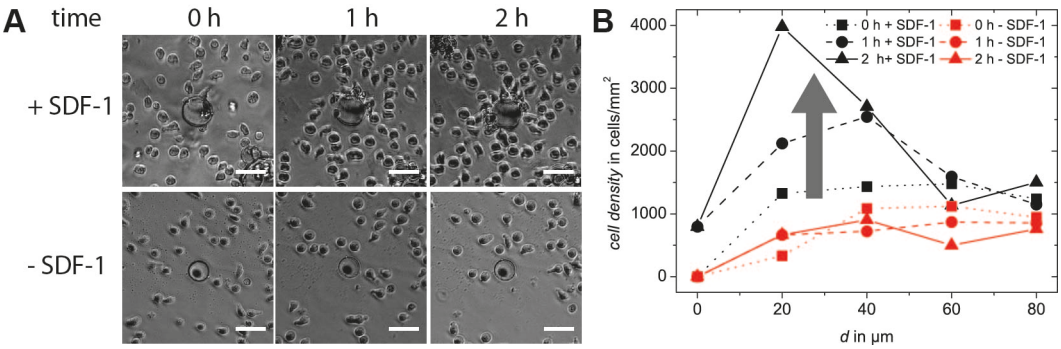

Figure 6: SDF-1 gradient attracts FDCPmix cells. A) Time series of bright field microscopy images of FDCP-Mix cells next to a SDF-1 laden µ-bead (upper row) and an empty bead (bottom row). FDCPmix cells only migrate towards the SDF-1 source (scale bar: 40 µm). **B)** Cell density in dependence on distance to µ-bead *d* at different time points. Cell density was analyzed from time series shown in **A)**. The arrow indicates sequential density profiles.

A further test within a cell environment resembling more closely the *in vivo* situation of the bone marrow was performed inside 3D collagen I networks using freshly isolated murine HSPC (Sca-1$^+$ Lin$^-$ CD150$^+$ CD48$^-$). The SDF-1 laden µ-beads were present during collagen network reconstitution and positioned in the lower third of the network layer (approx. total thickness 300 µm) due to sedimentation during the reconstitution phase. HSPC were seeded on top of the collagen networks. The cells needed around 8 h to reach the µ-bead level. Afterwards we investigated the attraction of these cells toward an SDF-1 gradient using video microscopy charting the whole 3D collagen network volume. Figure 7 (see also supplementary movie S1_HSPC_bead.avi) shows a migrating HSPC that was attracted by the SDF-1 gradient. The cell remained within the immediate vicinity (< 50 µm) of the µ-bead over 8 h, finally being strongly attracted by the chemokine source. We noted that not all cells that reached the bead level migrated toward the µ-beads. This behavior is not unexpected due to the short-range character of the gradients and the cell population heterogeneity with respect to CXCR4 expression. The latter issue is well-known from other experiments using trans-well assays in which only small fractions of the cell population respond to the chemokine, irrespective of whether the SDF-1 source is in solution [42] or being released from a hydrogel [60]. Furthermore, cells' indifference toward SDF-1 sources was reported to be even more pronounced at low SDF-1 concentrations, comparable to those used in this work [42,60]. By comparing our results to theoretically calculated SDF-1 gradients (Figure 5C) at a distance of 50 µm, we can conclude that at least a subpopulation of HSPC sense SDF-1 concentration levels of < 1 pg/ml and respond by migrating towards the source.

In summary, the experiments using SDF-1 showed that our µ-bead based system delivers functional short-range SDF-1 gradients that instruct chemotactic cell migration. Two hematopoietic cell types, namely the FDCPmix cell line and primary murine HSPC, showed sensitivity for these gradients down to 2 pg/ml or < 1 pg/ml concentrations, respectively, both in 2D and 3D cell migration. Further experiments on a single cell level are needed to reveal in more detail the impact of such gradients in heterogeneous cell populations.

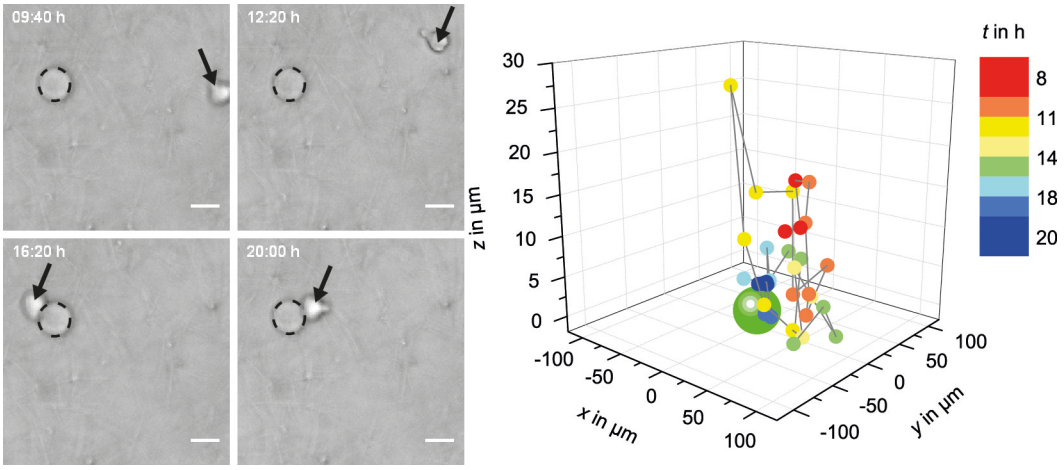

Figure 7: SDF-1 gradient attracts murine HSPC within a 3D collagen network. Time evolution (upper part of image) of HSPC migration (arrow) in a 3D collagen I network containing SDF-1 laden µ-beads (dashed circle). HSPC were initially seeded on top of the network and reached bead level after around 8 h. The time series shows HSPC attracted by the short-range SDF-1 gradient (scale bar: 20 µm). The positions of the cell including the last one in close vicinity of the µ-bead (green) are shown in different colors for increasing time. The full time series is shown in a supplementary movie (S1_HSPC_bead.avi).

Conclusion

We present a microparticle-based release system to mimic short-range paracrine cell-cell interactions. Functionalized and cytokine-laden agarose microparticles were used as surrogates of cytokine-releasing cells thereby establishing short-range cytokine gradients over a distance of some tens of micrometers. Using GAG as native binding partners of the cytokines as well as various cytokine loading concentrations, release rate and concentration levels of the cytokine gradients could be adjusted to mimic *in vivo* situations. A functional validation of the system was provided by the chemotaxis of HSPC toward SDF-1-laden microparticles. The system offers capability for long-term studies on single cell level *in vitro* and thereby will help to unravel cell fate decisions within heterogeneous cell populations in dependence on time and local position within short-range gradients of soluble paracrine signals of neighboring cells.

Acknowledgements

The authors acknowledge the support of grants from ESF 'European Social Funds' and Free State of Saxony (SAB, grant: 100140482), from EFRE and Free State of Saxony (SAB, grant: 100144684), from Deutsche Forschungsgemeinschaft (DFG, grant: SFB-TRR67/B10,A4,A10 and INST 268/293-1 FUGG) and from Human Frontier Science Program Organisation (HFSPO RGP0051/2011). We further acknowledge use of the imaging facility in the Magin lab, supported by DFG INST 68/230-1 to Thomas Magin and the imaging facility of the Biotec at TU Dresden. We thank Andreas Müller, Christina Müller and Liv Kalbitzer for fruitful discussions.

References

[1] J.B. Gurdon, P.Y. Bourillot, Morphogen gradient interpretation, Nature 413 (2001) 797–803.

[2] T. Tabata, Y. Takei, Morphogens, their identification and regulation, Development 131 (2004) 703–712.

[3] P. Müller, K.W. Rogers, B.M. Jordan, J.S. Lee, D. Robson, S. Ramanathan, A.F. Schier, Differential diffusivity of Nodal and Lefty underlies a reaction-diffusion patterning system, Science 336 (2012) 721–724.

[4] M. Strigini, S.M. Cohen, A Hedgehog activity gradient contributes to AP axial patterning of the Drosophila wing, Development 124 (1997) 4697–4705.

[5] D. Nellen, R. Burke, G. Struhl, K. Basler, Direct and long-range action of a DPP morphogen gradient, Cell 85 (1996) 357–368.

[6] A.T. Melvin, E.S. Welf, Y. Wang, D.J. Irvine, J.M. Haugh, In chemotaxing fibroblasts, both high-fidelity and weakly biased cell movements track the localization of PI3K signaling, Biophysical Journal 100 (2011) 1893–1901.

[7] J.J. Tomasek, G. Gabbiani, B. Hinz, C. Chaponnier, R.A. Brown, Myofibroblasts and mechano-regulation of connective tissue remodelling, Nature reviews. Molecular Cell Biology 3 (2002) 349–363.

[8] S.A. Eccles, Targeting key steps in metastatic tumour progression, Current Opinion in Genetics & Development 15 (2005) 77–86.

[9] N. Barker, S. Bartfeld, H. Clevers, Tissue-resident adult stem cell populations of rapidly self-renewing organs, Cell Stem Cell 7 (2010) 656–670.

[10] R. Schofield, The relationship between the spleen colony-forming cell and the haemopoietic stem cell, Blood cells 4 (1978) 7–25.

[11] D.T. Scadden, The stem-cell niche as an entity of action, Nature 441 (2006) 1075–1079.

[12] N. Barker, M. van de Wetering, H. Clevers, The intestinal stem cell, Genes & Development 22 (2008) 1856–1864.

[13] V. Jaks, N. Barker, M. Kasper, J.H. van Es, H.J. Snippert, H. Clevers, R. Toftgard, Lgr5 marks cycling, yet long-lived, hair follicle stem cells, Nature Genetics 40 (2008) 1291–1299.

[14] M. Inaba, M. Buszczak, Y.M. Yamashita, Nanotubes mediate niche-stem-cell signalling in the Drosophila testis, Nature 523 (2015) 329–332.

[15] C.J. Eaves, Hematopoietic stem cells: concepts, definitions, and the new reality, Blood 125 (2015) 2605–2613.

[16] P.E. Boulais, P.S. Frenette, Making sense of hematopoietic stem cell niches, Blood 125 (2015) 2621–2629.

[17] T. Ara, K. Tokoyoda, T. Sugiyama, T. Egawa, K. Kawabata, T. Nagasawa, Long-term hematopoietic stem cells require stromal cell-derived factor-1 for colonizing bone marrow during ontogeny, Immunity 19 (2003) 257–267.

[18] S.J. Morrison, D.T. Scadden, The bone marrow niche for haematopoietic stem cells, Nature 505 (2014) 327–334.

[19] T. Nagasawa, K. Tachibana, T. Kishimoto, A novel CXC chemokine PBSF/SDF-1 and its receptor CXCR4: their functions in development, hematopoiesis and HIV infection, Seminars in immunology 10 (1998) 179–185.

[20] J.M. Burns, B.C. Summers, Y. Wang, A. Melikian, R. Berahovich, Z. Miao, M.E.T. Penfold, M.J. Sunshine, D.R. Littman, C.J. Kuo, K. Wei, B.E. McMaster, K. Wright, M.C. Howard, T.J. Schall, A novel chemokine receptor for SDF-1 and I-TAC involved in cell survival, cell adhesion, and tumor development, The Journal of Experimental Medicine 203 (2006) 2201–2213.

[21] U. Naumann, E. Cameroni, M. Pruenster, H. Mahabaleshwar, E. Raz, H.-G. Zerwes, A. Rot, M. Thelen, CXCR7 functions as a scavenger for CXCL12 and CXCL11, PloS one 5 (2010) e9175.

[22] D.R. Coombe, Biological implications of glycosaminoglycan interactions with haemopoietic cytokines, Immunology and Cell Biology 86 (2008) 598–607.

[23] B. Mulloy, C.C. Rider, Cytokines and proteoglycans: an introductory overview, Biochemical Society Transactions 34 (2006) 409–413.

[24] A. Zieris, R. Dockhorn, A. Röhrich, R. Zimmermann, M. Müller, P.B. Welzel, M.V. Tsurkan, J.-U. Sommer, U. Freudenberg, C. Werner, Biohybrid networks of selectively desulfated glycosaminoglycans for tunable growth factor delivery, Biomacromolecules 15 (2014) 4439–4446.

[25] S. Prokoph, E. Chavakis, K.R. Levental, A. Zieris, U. Freudenberg, S. Dimmeler, C. Werner, Sustained delivery of SDF-1alpha from heparin-based hydrogels to attract circulating pro-angiogenic cells, Biomaterials 33 (2012) 4792–4800.

[26] A.B. Brennan, C.M. Kirschner, Bio-inspired materials for biomedical engineering, Wiley, Hoboken, NJ, USA, 2014.

[27] M.J. Kiel, Ö.H. Yilmaz, T. Iwashita, O.H. Yilmaz, C. Terhorst, S.J. Morrison, SLAM family receptors distinguish hematopoietic stem and progenitor cells and reveal endothelial niches for stem cells, Cell 121 (2005) 1109–1121.

[28] S. Boyden, The chemotactic effect of mixtures of antibody and antigen on polymorphonuclear leucocytes, The Journal of Experimental Medicine 115 (1962) 453–466.

[29] T.M. Keenan, A. Folch, Biomolecular gradients in cell culture systems, Lab on a Chip 8 (2008) 34–57.

[30] V.V. Abhyankar, M.A. Lokuta, A. Huttenlocher, D.J. Beebe, Characterization of a membrane-based gradient generator for use in cell-signaling studies, Lab on a Chip 6 (2006) 389–393.

[31] K. Franke, J. Sapudom, L. Kalbitzer, U. Anderegg, T. Pompe, Topologically defined composites of collagen types I and V as in vitro cell culture scaffolds, Acta Biomaterialia 10 (2014) 2693–2702.

[32] J. Sapudom, S. Rubner, S. Martin, T. Kurth, S. Riedel, C.T. Mierke, T. Pompe, The phenotype of cancer cell invasion controlled by fibril diameter and pore size of 3D collagen networks, Biomaterials 52 (2015) 367–375.

[33] J. Sapudom, S. Rubner, S. Martin, S. Thoenes, U. Anderegg, T. Pompe, The interplay of fibronectin functionalization and TGF-β1 presence on fibroblast proliferation, differentiation and migration in 3D matrices, Biomaterials Science 3 (2015) 1291–1301.

[34] S.J. Habib, B.-C. Chen, F.-C. Tsai, K. Anastassiadis, T. Meyer, E. Betzig, R. Nusse, A localized Wnt signal orients asymmetric stem cell division in vitro, Science 339 (2013) 1445–1448.

[35] Y. Wang, D.J. Irvine, Engineering chemoattractant gradients using chemokine-releasing polysaccharide microspheres, Biomaterials 32 (2011) 4903–4913.

[36] Y. Wang, D.J. Irvine, Convolution of chemoattractant secretion rate, source density, and receptor desensitization direct diverse migration patterns in leukocytes, Integrative Biology 5 (2013) 481–494.

[37] V. Hintze, S. Moeller, M. Schnabelrauch, S. Bierbaum, M. Viola, H. Worch, D. Scharnweber, Modifications of hyaluronan influence the interaction with human bone morphogenetic protein-4 (hBMP-4), Biomacromolecules 10 (2009) 3290–3297.

[38] S. Rother, J. Salbach-Hirsch, S. Moeller, T. Seemann, M. Schnabelrauch, L.C. Hofbauer, V. Hintze, D. Scharnweber, Bioinspired collagen/glycosaminoglycan-based cellular microenvironments for tuning osteoclastogenesis, ACS Applied Materials & Interfaces (2015).

[39] J. Salbach-Hirsch, N. Ziegler, S. Thiele, S. Moeller, M. Schnabelrauch, V. Hintze, D. Scharnweber, M. Rauner, L.C. Hofbauer, Sulfated glycosaminoglycans support osteoblast functions and concurrently suppress osteoclasts, Journal of Cellular Biochemistry 115 (2014) 1101–1111.

[40] L. Baumann, A.G. Beck-Sickinger, Identification of a potential modification site in human stromal cell-derived factor-1, Biopolymers 94 (2010) 771–778.

[41] L. Baumann, M. Steinhagen, A. Beck-Sickinger, Preparation of C-terminally modified chemokines by expressed protein ligation, in: K.J. Jensen, P.T. Shelton, S.L. Pedersen (Eds.), Peptide synthesis and applications, Humana Press, Totowa, New Jersey, 2013, pp. 103–118.

[42] K. Bellmann-Sickert, L. Baumann, A.G. Beck-Sickinger, Selective labelling of stromal cell-derived factor 1α with carboxyfluorescein to study receptor internalisation, Journal of Peptide Science 16 (2010) 568–574.

[43] S. Brew, K. Ingram, Purification of human plasma fibronectin, Journal of Tissue Culture Methods 16 (1994) 197–199.

[44] L. Poulouin, O. Gallet, M. Rouahi, J.M. Imhoff, Plasma fibronectin: three steps to purification and stability, Protein Expression and Purification 17 (1999) 146–152.

[45] I. Capila, R.J. Linhardt, Heparin-protein interactions, Angewandte Chemie (International ed. in English) 41 (2002) 391–412.

[46] J. Crank, The mathematics of diffusion, 2nd ed., Clarendon Press, Oxford [Eng], 1975.

[47] J. Siepmann, F. Lecomte, R. Bodmeier, Diffusion-controlled drug delivery systems: calculation of the required composition to achieve desired release profiles, Journal of Controlled Release 60 (1999) 379–389.

[48] O. Krichevsky, G. Bonnet, Fluorescence correlation spectroscopy: the technique and its applications, Reports on Progress in Physics 65 (2002) 251–297.

[49] P. Kapusta, Application note: Absolute diffusion coefficients. Compilation of Reference Data for FCS Calibration, Berlin, 2010.

[50] A. Pierce, Y. Lu, H.G. Hamzah, S. Thompson, P.J. Owen-Lynch, A.D. Whetton, E. Spooncer, Differential effect of leukaemogenic tyrosine kinases on cell motility is governed by subcellular localisation, British Journal of Haematology 133 (2006) 345–352.

[51] S. Petrovic, M. Cross, A.M. Muller, Differentiation potential of FDCPmix cells following injection into blastocysts, Cells, Tissues, Organs 178 (2004) 78–86.

[52] E. Spooncer, T.M. Dexter, Culturing primitive hemopoietic cells: Long-Term Mouse Marrow Cultures and the Establishment of Factor-Dependent (FDCP-Mix) Hemopoietic Cell Lines, Methods in Molecular Biology (Clifton, N.J.) 5 (1990) 277–288.

[53] J. Duo, J.A. Stenken, Heparin-immobilized microspheres for the capture of cytokines, Analytical and Bioanalytical Chemistry 399 (2011) 773–782.

[54] O. Arlov, F.L. Aachmann, A. Sundan, T. Espevik, G. Skjåk-Bræk, Heparin-like properties of sulfated alginates with defined sequences and sulfation degrees, Biomacromolecules 15 (2014) 2744–2750.

[55] R.E. Canfield, The amino acid sequence of egg white lysozyme, Journal of Biological Chemistry 238 (1963) 2698–2707.

[56] L.R. Wetter, H.F. Deutsch, Immunological studies on egg white proteins. IV. Immunochemical and physical studies of lysozyme, Journal of Biological Chemistry 192 (1951) 237–242.

[57] S. Koutsopoulos, L.D. Unsworth, Y. Nagai, S. Zhang, Controlled release of functional proteins through designer self-assembling peptide nanofiber hydrogel scaffold, Proceedings of the National Academy of Sciences of the United States of America 106 (2009) 4623–4628.

[58] V. Hintze, A. Miron, S. Moeller, M. Schnabelrauch, H.-P. Wiesmann, H. Worch, D. Scharnweber, Sulfated hyaluronan and chondroitin sulfate derivatives interact differently with human transforming growth factor-β1 (TGF-β1), Acta Biomaterialia 8 (2012) 2144–2152.

[59] H. Mach, D.B. Volkin, C.J. Burke, C.R. Middaugh, R.J. Linhardt, J.R. Fromm, D. Loganathan, L. Mattsson, Nature of the interaction of heparin with acidic fibroblast growth factor, Biochemistry 32 (1993) 5480–5489.

[60] L. Baumann, S. Prokoph, C. Gabriel, U. Freudenberg, C. Werner, A.G. Beck-Sickinger, A novel, biased-like SDF-1 derivative acts synergistically with starPEG-based heparin hydrogels and improves eEPC migration in vitro, Journal of Controlled Release 162 (2012) 68–75.

[61] W. Norde, Protein adsorption at solid surfaces: A thermodynamic approach, Pure and Applied Chemistry 66 (1994).

[62] R. Sadir, F. Baleux, A. Grosdidier, A. Imberty, H. Lortat-Jacob, Characterization of the stromal cell-derived factor-1α-heparin complex, Journal of Biological Chemistry 276 (2001) 8288–8296.

[63] A.I. Liapis, B.A. Grimes, K. Lacki, I. Neretnieks, Modeling and analysis of the dynamic behavior of mechanisms that result in the development of inner radial humps in the concentration of a single adsorbate in the adsorbed phase of porous adsorbent particles observed in confocal scanning laser microscopy experiments: diffusional mass transfer and adsorption in the presence of an electrical double layer, Journal of Chromatography A 921 (2001) 135–145.

[64] F.-X. Yu, W.-J. Hu, B. He, Y.-H. Zheng, Q.-Y. Zhang, L. Chen, Bone marrow mesenchymal stem cells promote osteosarcoma cell proliferation and invasion, World Journal of Surgical Oncology 13 (2015) 52.

[65] R.G. Endres, N.S. Wingreen, Accuracy of direct gradient sensing by single cells, Proceedings of the National Academy of Sciences of the United States of America 105 (2008) 15749–15754.